Biomaterials 163 (2018) 55–66

Contents lists available at ScienceDirect

Biomaterials

journal homepage: www.elsevier.com/locate/biomaterials

Photo-tearable tape close-wrapped upconversion nanocapsules for near-infrared modulated efficient siRNA delivery and therapy

Yue Zhang [a], Kewei Ren [a], Xiaobo Zhang [a], Zhicong Chao [a], Yuqin Yang [a], Deju Ye [a], Zhihui Dai [b], Ying Liu [a, *], Huangxian Ju [a, *]

[a] State Key Laboratory of Analytical Chemistry for Life Science, School of Chemistry and Chemical Engineering, Nanjing University, Nanjing, 210023, PR China

[b] Jiangsu Collaborative Innovation Centre of Biomedical Functional Materials and Jiangsu Key Laboratory of Biofunctional Materials, School of Chemistry and Materials Science, Nanjing Normal University, Nanjing, 210023, PR China

ARTICLE INFO

Article history:
Received 30 October 2017
Received in revised form
6 February 2018
Accepted 8 February 2018
Available online 9 February 2018

Keywords:
Upconversion nanoparticles
Photocleavage
SiRNA delivery
Endosomal escape
Gene silencing

ABSTRACT

RNA interference (RNAi) has become an appealing therapeutic approach for cancer and other diseases. One key challenge is the effective protection of these small fragile biomolecules against complicated physiological environments as well as efficient on-demand release. Here we design a photo-tearable polymer tape close-wrapped nanocapsule for efficient NIR modulated siRNA delivery. The photo-tearable nanocapsules comprise core-shell upconversion nanoparticles (UCNPs) coated with mesoporous silica layer for loading of photosensitizer hypocrellin A (HA) and small interfering RNA (siRNA) against polo-like kinase 1 (PLK1), and covalently bound thin membranes of polyethylene glycol (PEG) *via* a synthesized photocleavable linker (PhL). Upon irradiation at 980 nm, the UCNPs produce UV emissions to break PhL and tear out PEG membrane for siRNA release, and blue emissions to activate HA for generating reactive oxygen species (ROS). The close PEG membrane wrapping not only guarantees the efficient intracellular photocleavage, but also extends the circulation time and protects the loaded cargos from leakage and degradation. The ROS assists endosomal escape of the loaded cargos, therefore effectively improves the gene silencing efficiency and the suppressions of cell proliferation *in vitro* and tumor growth *in vivo*. The proposed photo-tearable tape-wrapped nanocapsules have promising potential application in precision medicine.

1. Introduction

RNA interference (RNAi), which utilizes exogenous small interfering RNA (siRNA) to specifically inhibit target gene expression [1–3], has become a tremendously appealing approach for innovative therapy [4]. However, one of the challenges for the broad clinical application of RNAi remains the efficient delivery of these small fragile biomolecules in target cells. The delivery vehicles must protect siRNA well from leakage and degradation in extracellular biological fluid, and controllably release siRNA in the cytoplasm of target cells [3,5]. Packing siRNA with nanoparticles, such as mesoporous silica [6], gold nanoshells [7], and polymers [8,9], has extended siRNA half-life in blood, enhanced tumor-specific cellular uptake and improved the gene transfection efficiency [10,11]. However, siRNA on the outer surface of nanoparticles is still exposed to the complicated physiological environment, which makes it amenable to RNase degradation [12,13]. Although mesoporous silica nanoparticles have been used to entirely encapsulate siRNA [14], it is difficult to turn the intracellular release of siRNA.

On-demand delivery and release using external stimuli are an important way for precise therapy since external triggers allow for better duration and dosage controls [15–17]. Light stands out among different external stimuli due to its noninvasiveness, easy generation and manipulation, and controllability with high spatiotemporal precision [18–20]. Some photoactive molecules containing *o*-nitrobenzyl moieties can be irreversibly cleaved under irradiation [21], and have been extensively applied for precise drug delivery [22] and optogenetic applications [23]. However, UV light is generally required for most of the photoreactions, which leads to phototoxicity [24] and quick attenuation in body tissues [25], and imposes the restrictions on its *in vivo* applications. Thus near-infrared (NIR) irradiation has attracted considerable attention in

* Corresponding authors.
E-mail addresses: yingliu@nju.edu.cn (Y. Liu), hxju@nju.edu.cn (H. Ju).

https://doi.org/10.1016/j.biomaterials.2018.02.019
0142-9612/

noninvasive therapy due to its significantly less damage to living tissues, remarkably deeper light penetration, and low autofluorescence background [26,27]. By combining the special natures of lanthanide-doped upconversion nanoparticles (UCNPs), which can adsorb two or more low energy photons to give out a higher energy photon [28], NIR irradiation can be upconverted to UV and visible radiations [29–32]. Accordingly, photoactivated molecules modified DNA [33], drugs [34,35] or targeting probes [36] have been incorporated with UCNPs to regulate intracellular gene expression and achieve light-activated cancer therapy, and incorporation of UCNPs with photodegradable polymers has been witnessed a rapid growth for drug delivery [37–39] and controllable macromolecules release [40–42].

Generally, the UCNPs and photocleavage sites are randomly distributed in the photodegradable polymers [37,39–41], which leads to a long travel distance of the upconverted UV light to reach all photocleavable cross-links, therefore lowers the utilization efficiency of light for intracellular application. To improve the photocleavage efficiency, here a photocleavable linker (PhL) was synthesized to covalently link polyethylene glycol (PEG) polymer to mesoporous silica coated UCNPs for design of a photo-tearable polymer "tape" and controllable release of siRNA from UCNP nanocapsules (Scheme 1a). The siRNA could be conveniently loaded on the surface of PhL modified silica *via* electrostatic adsorption, and the subsequent PEG encapsulation effectively extended the circulation time [43] and protected the loaded cargos from leakage and degradation. Upon irradiation at 980 nm, UCNPs produced two emissions at 345 and 365 nm to cleave the PhL and thus tore off the polymer tape to release siRNA intracellularly. However, this PEGylated system lacked the ability of membrane disruption for endosomal escape of siRNA to perform its gene silencing function. Thus a photosensitizer, hypocrellin A (HA), was loaded in the pores of mesoporous silica, which was activated by the upconverted emissions of UCNPs at 455 and 475 nm and generated reactive oxygen species (ROS). The ROS not only disrupted the endosomal membrane and liberated siRNA into cytoplasm (Scheme 1b) to boost the gene therapy efficiency, but also destructed cellular organelles to assist cell apoptosis. The designed photo-tearable tape-wrapped UCNP nanocapsules provided a universal strategy for efficient NIR-assisted gene therapy.

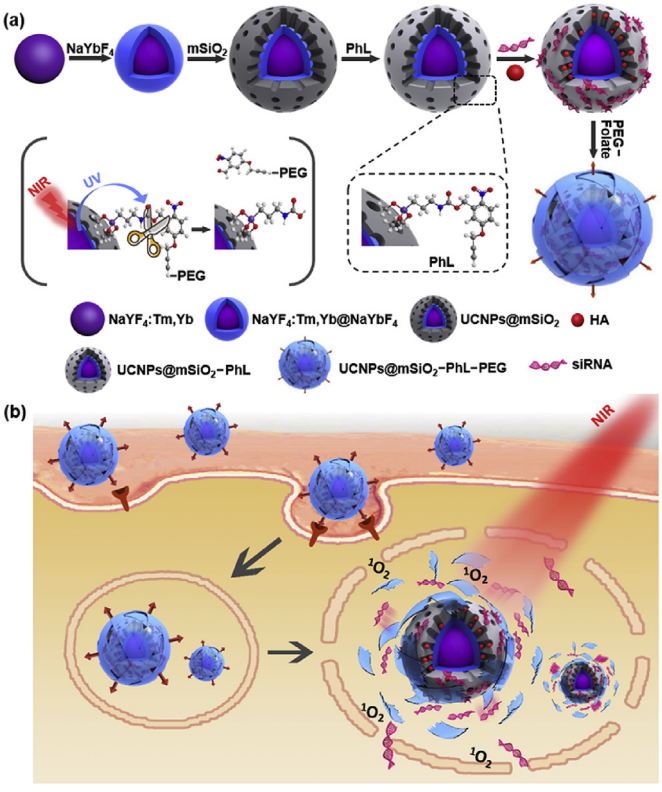

Scheme 1. Schematic illustrations of (a) synthesis of UCNP nanocapsules, and (b) folate receptor-mediated cellular uptake and NIR modulated intracellular siRNA delivery and therapy.

2. Materials and methods

2.1. Materials and apparatus

Anhydrous yttrium chloride (YCl_3) (99.9%), anhydrous ytterbium chloride ($YbCl_3$) (99.9%) and anhydrous thulium chloride ($TmCl_3$) (99.9%) were purchased from Sigma-Aldrich (USA). Sodium hydroxide, ammonium fluoride, cyclohexene, oleic acid (OA), 1-octadecene (ODE), (3-aminopropyl) triethoxysilane (APTES), cetyltrimethylammonium bromide (CTAB), tetraethylorthosilicate (TEOS), Cu(II) sulfate, L-ascorbic acid, potassium carbonate (K_2CO_3), N, N′-dimethylformamide (DMF), dimethyl sulfoxide (DMSO), propargyl bromide, ethyl acetate (EtOAc), sodium sulfate (Na_2SO_4), petroleum ether, tetrahydrofuran (THF), triethylamine (Et_3N), methanol (MeOH), sodium borohydride ($NaBH_4$), 5-hydroxy-2-nitro-benzaldehyde (HNB), N, N′-disuccinimidyl carbonate (DSC), 1,3-diphenylisobenzofuran (DPBF) and acetonitrile (MeCN) were purchased from Aladin Ltd (Shanghai, China). 4-Dimethylaminopyridine (DMAP) was purchased from Adamas Reagent, Ltd. (Shanghai, China). Hypocrellin A (HA) was purchased from Biopurify (Chengdu, China). Four-armed polyethylene glycol modified with azido (PEG) (MW 2000) and two-armed polyethylene glycol modified with both azido and folate (PEG(FA)) or FITC (PEGF) (MW 2000) were purchased from Toyongbio (Shanghai, China). LysoTracker Red was purchased from Invitrogen (Carlsbad, CA, USA). Annexin V-FITC apoptosis detection kit and dihydroethidium were purchased from Keygen Biotech (Nanjing, China). RNA extraction kit, PrimeScript RT reagent kit and SYBR premix EX Taq kit were purchased from Takara (Dalian, China). PLK1 ELISA kit was purchased from Jin Yibai Biological Technology (Nanjing, China). PLK1 siRNA was purchased from GenePharma Ltd (Shanghai, China). The siRNA sequences were as follows:

siRNA: 5′-UGAAGAAGAUCACCCUCCUUAdTdT-3′,
siRNA-FAM: 5′-FAM-UGAAGAAGAUCACCCUCCUUAdTdT-3′,
siRNA-Cy5: 5′-Cy5-UGAAGAAGAUCACCCUCCUUAdTdT-3′,
Antisense: 5′-UAAGGAGGGUGAUCUUCUUCA-3′,
BHQ-antisense: 5′-UAAGGAGGGUGAUCUUCUUCA-BHQ-3'.

Transmission electron microscopic (TEM) images were captured on JEM-2100 transmission electron microscope (JEOL Ltd., Japan). Dynamic light scattering (DLS) was conducted on ZetaPlus 90 Plus/BI-MAS (Brook haven, USA). Zeta potential analysis was conducted on Nano-Z Zetasizer (Malvern, UK). The UV–Vis absorption spectra were performed with Nanodrop-2000C UV–Vis spectrophotometer (Nanodrop, USA). Flow cytometric analysis was conducted on Coulter FC-500 flow cytometer (Beckman-Coulter, USA). The fluorescence spectra were acquired on F-7000 spectrofluorophotometer (HITACHI, Japan). The cell images were obtained on TCS SP5 confocal laser scanning microscope (CLSM) (Leica, Germany). Upconversion luminescence (UCL) spectra were collected on ZolixScan ZLX-UPL spectrometer with an external continuous-wave laser (980 nm) as the excitation source. MTT and ELISA assays were conducted on Hitachi/Roche System Cobas 6000

(Bio-Rad, USA). RT-qPCR was conducted on StepOne Real-Time PCR System (Thermo Fisher Scientific, USA).

2.2. Synthesis of PhL

After 5-hydroxy-2-nitrobenzaldehyde (1.67 g, 10.0 mmol, 1.0 equiv.) was mixed with K_2CO_3 (2.76 g, 20.0 mmol, 2.0 equiv.) and propargyl bromide (2.38 g, 2.0 equiv.) in DMF (30 mL) to react overnight under stirring at room temperature, the mixture was diluted with water (100 mL) and extracted with EtOAc (3 × 50 mL). The combined organic layer was then washed with brine (50 mL), and dried over Na_2SO_4. After removing solvent under reduced pressure, the crude product was purified by column chromatography (petroleum ether/EtOAc gradient: 10/1) to give compound **1**, 2-nitro-5-(prop-2-yn-1-yloxy)benzaldehyde (1.94 g, 9.46 mmol, 95%). ^{1}H NMR (400 MHz, $CDCl_3$, δ): 10.39 (s, 1H, CHO), 8.12 (d, J = 9.0 Hz, 1H; Ar H), 7.35 (d, J = 2.8 Hz, 1H; Ar H), 7.22 (dd, J = 9.0, 2.8 Hz, 1H; Ar H), 4.82 (d, J = 2.3 Hz, 2H; CH_2), 2.60 (t, J = 2.2 Hz, 1H; CH). ^{13}C NMR (101 MHz, $CDCl_3$, δ): 188.13(C═O), 161.59(C4), 142.64(C4), 133.98(C4), 127.06(C3), 119.08(C3), 114.46(C3), 77.17(C4), 76.52(C3), 56.52(C2).

After compound **1** (1.02 g, 5.0 mmol, 1.0 equiv.) was dissolved in the mixture of THF (20 mL) and MeOH (20 mL), $NaBH_4$ (0.380 g) was added at 0 °C to stir for 20 min at room temperature, and the mixture was then diluted with water (100 mL) and extracted with EtOAc (3 × 50 mL). The combined organic layer was washed with brine (50 mL) and dried over Na_2SO_4, and the solvent was removed under reduced pressure to give compound **2**, (2-nitro-5-(prop-2-yn-1-yloxy)phenyl)methanol (1.01 g, 4.9 mmol, 98%). ^{1}H NMR (400 MHz, DMSO-d_6, δ): 8.19 (d, J = 9.1 Hz, 1H; Ar H), 7.44 (d, J = 2.9 Hz, 1H; Ar H), 7.13 (dd, J = 9.1, 2.9 Hz, 1H; Ar H), 5.63 (t, J = 5.5 Hz, 1H; OH), 5.01 (d, J = 2.4 Hz, 2H; CH_2), 4.89 (d, J = 5.5 Hz, 2H; CH_2), 3.71 (t, J = 2.4 Hz, 1H; CH). ^{13}C NMR (101 MHz, DMSO-d6, δ): 162.38(C4), 143.10(C4), 140.84(C4), 128.24(C3), 114.72(C3), 114.04(C3), 79.97(C4), 79.25(C3), 61.04(C2), 57.06(C2).

Compound **2** (1.03 g, 5.0 mmol, 1.0 equiv.) was mixed with bis(2,5-dioxopyrrolidin-1-yl) carbonate (1.53 g, 6.0 mmol, 1.2 equiv.), Et_3N (1.01 g, 1.0 mmol, 2.0 equiv.) in MeCN (20 mL) and stirred at room temperature overnight. After removing solvent under reduced pressure, the crude product was purified by column chromatography (petroleum ether/EtOAc gradient: 3/1) to give the **PhL**, 2,5-dioxopyrrolidin-1-yl (2-nitro-5-(prop-2-yn-1-yloxy) benzyl) carbonate (1.00 g, 2.87 mmol, 57%). ^{1}H NMR (400 MHz, $CDCl_3$, δ): 8.26 (d, J = 9.2 Hz, 1H; Ar H), 7.24 (d, J = 2.6 Hz, 1H; Ar H), 7.05 (dd, J = 9.2, 2.8 Hz, 1H; Ar H), 5.82 (s, 2H, CH_2), 4.87 (d, J = 2.4 Hz, 2H; CH_2), 2.86 (s, 4H, CH_2), 2.63 (t, J = 2.4 Hz, 1H; CH). ^{13}C NMR (101 MHz, $CDCl_3$, δ): 168.38(C═O), 162.13(C═O), 151.31(C4), 140.03(C4), 133.53(C4), 128.04(C3), 115.09(C3), 112.98(C3), 77.06(C4), 76.87(C3), 69.00(C2), 56.51(C2), 25.45(C2).

2.3. Synthesis of $NaYF_4$:Tm,Yb UCNPs

According to the previous report [44], YCl_3 (0.695 mmol), $YbCl_3$ (0.300 mmol) and $TmCl_3$ (0.005 mmol) were firstly mixed with oleic acid (6 mL) and 1-octadecene (15 mL), and heated to 150 °C under vacuum and stirring for 40 min to completely remove residual water and oxygen. After cooling down to room temperature, methanol solution (10 mL) of NH_4F (148 mg) and NaOH (100 mg) was added dropwise into the mixture under stirring for 30 min. The reaction mixture was then heated and kept at 110 °C for 15 min and 300 °C for 80 min under the nitrogen atmosphere. Afterward the mixture was naturally cooled down to room temperature to get the $NaYF_4$:Tm,Yb UCNPs. The resulting UCNPs were precipitated with acetone, repeatedly washed with ethanol, and re-dispersed in 10 mL cyclohexane for further use.

2.4. Synthesis of $NaYF_4$:Tm,Yb@$NaYbF_4$ core-shell UCNPs

The synthesis of core-shell UCNPs referred to the previous report [45]. After $YbCl_3$ (0.80 mmol) was mixed with oleic acid (6 mL) and 1-octadecene (15 mL) and heated to 150 °C under vacuum and stirring for 40 min, a transparent solution was obtained and cooled down to 40 °C. The above synthesized $NaYF_4$:Tm,Yb UCNPs (10 mL, cyclohexane) were then slowly added into the mixture and heated to 80 °C for a while to completely remove cyclohexane and subsequently cooled down to 50 °C. Subsequently, the methanol solution (10 mL) of NH_4F (118 mg) and NaOH (80 mg) was added under stirring for 30 min at room temperature, and the reaction mixture was finally heated and kept at 110 °C for 15 min and 300 °C for 80 min under a nitrogen atmosphere to get the $NaYF_4$:Tm,Yb@$NaYbF_4$ core-shell UCNPs. The resulting core-shell UCNPs were precipitated with acetone, repeatedly washed with ethanol, and re-dispersed in chloroform for further use.

2.5. Modification of core-shell UCNPs with $mSiO_2$ shell

The modification of core-shell UCNPs with $mSiO_2$ shell referred to the previous report [46,47]. In brief, after the cyclohexane solution (2 mL) of $NaYF_4$:Tm,Yb@$NaYbF_4$ core-shell UCNPs (10 mg) was mixed with 5 mg mL^{-1} CTAB aqueous solution (20 mL), and vigorously stirred at room temperature overnight, a clear UCNPs/CTAB solution was obtained, which was then mixed with water (40 mL), ethanol (6 mL) and 2 M NaOH aqueous solution (300 μL), heated to 70 °C under stirring, and followed by adding 340 μL TEOS and 60 μL APTES dropwise. The mixture solution was kept reaction for 2 h, centrifuged and repeatedly washed with ethanol, followed by continuously reacting with ethanol solution (100 mL) of NH_4NO_3 (0.6 g) at 60 °C for 2 h to remove the CTAB. The as-obtained UCNPs@$mSiO_2$ was centrifuged and washed with ethanol, and dispersed in ethanol.

2.6. Preparation of HA and siRNA loaded UCNPs@$mSiO_2$-PhL-PEG

After UCNPs@$mSiO_2$ (5 mg) was dispersed in DMSO (5 mL), 0.6% PhL DMSO solution (100 μL) and DMAP (2 mg) were added. The mixture was kept stirring overnight at room temperature in dark to obtain UCNPs@$mSiO_2$-PhL, which was centrifuged, washed with DMSO for three times, and re-dispersed in DMSO to kept away from light.

The loading of HA into the mesoporous silica of UCNPs@$mSiO_2$-PhL was performed by mixing 1 mg UCNPs@$mSiO_2$-PhL in 1 mL PBS with 2.5 mg mL^{-1} HA DMSO solution (20 μL) to stir overnight in dark. The product was centrifuged, washed with PBS, and redispersed in PBS. SiRNA was then loaded on the surface of UCNPs@$mSiO_2$-PhL *via* electrostatic interaction by adding 20 μM siRNA (80 μL) in 0.5 mg mL^{-1} HA-loaded UCNPs@$mSiO_2$-PhL aqueous solution (1 mL, PBS) to vibrate for 4 h, centrifuge and gently wash with PBS for two times. The as-prepared HA and siRNA co-loaded UCNPs were redispersed in PBS for PEG and PEG(FA) linkage.

PEG and PEG(FA) were covalently linked to UCNPs@$mSiO_2$-PhL through click reaction [20]. After UCNPs@$mSiO_2$-PhL (5 mg), 1% PEG aqueous solution (50 μL), 1% PEG(FA) aqueous solution (100 μL), 1 mM Cu(II) sulfate aqueous solution (20 μL) and 1 mM ascorbic acid aqueous solution (20 μL) were added into 10 mL PBS and kept stirring for 12 h at room temperature in dark, the obtained UCNPs@$mSiO_2$-PhL-PEG was centrifuged, washed twice with PBS, and re-dispersed in 1 mL PBS. 5 mg UCNPs@$mSiO_2$ was used instead of UCNPs@$mSiO_2$-PhL as the control group to verify the nonspecific adsorption of PEG and PEG(FA) on UCNPs.

To verify the serum stability of siRNA loaded on UCNP

nanocapsules, the self-quenched siRNA duplex structure tagged with FAM and BHQ was assembled to load on UCNPs@$mSiO_2$-PhL and UCNP nanocapsules. 450 nM siRNA duplex structure, UCNPs@$mSiO_2$-PhL and UCNP nanocapsules loaded with the same amount of siRNA duplex structure were separately dispersed in PBS containing 10% FBS, and incubated at 37 °C for 12 h. The fluorescence from FAM was then measured at different times under 480 nm excitation and 515 nm emission.

2.7. Photocleavage and siRNA release

The PhL degradation was verified by dispersing 1 mg UCNPs@$mSiO_2$-PhL in 200 μL DMSO to irradiate with 980-nm laser at 2 W cm^{-2} for different times. The resulting UCNPs@$mSiO_2$-PhL was centrifuged, washed with DMSO and redispersed in 200 μL DMSO for UV–Vis absorption measurements.

The photocleavage of PEG tape was verified with UCNPs@$mSiO_2$-PhL-PEGF, which was synthesized by mixing 300 μL PEGF (1% aqueous solution) with 5 mg UCNPs@$mSiO_2$-PhL according to the above procedure. After 1 mg UCNPs@$mSiO_2$-PhL-PEGF was dispersed in 200 μL PBS and irradiated with 980-nm laser at 2 W cm^{-2} over 180 min, the PEGF modified UCNPs were centrifuged, washed with water and redispersed in 200 μL PBS for fluorescence measurements.

To quantify siRNA release from UCNPs@$mSiO_2$-PhL-PEG, siRNA-FAM was loaded on UCNPs@$mSiO_2$-PhL-PEG and exposed to alternate NIR irradiations with 30 min-gap over 300 min. At different irradiation times, the siRNA-FAM loaded UCNPs solutions were centrifuged to measure the fluorescence intensity of supernatants for calculation of the siRNA release percentage.

2.8. Cell culture

HeLa cells were cultured in Dulbecco's modified Eagle's medium (DMEM, GIBCO) supplemented with 10% FBS, 1% Penicillin-Streptomycin Solution (100 μg mL^{-1}) at 37 °C in a humidified atmosphere containing 5% CO_2. Cell number was calculated using Countess® II automated cell counter (Invitrogen, USA).

2.9. ROS detection

After 5 mg mL^{-1} HA-loaded UCNPs@$mSiO_2$-PhL-PEG solution (1 mL) was mixed with 2.5 mM DPBF aqueous solution (50 μL) and irradiated with a 980-nm laser at 2 W cm^{-2}, the absorbances of DPBF in supernatant solutions over 80 min were monitored at 412 nm.

The intracellular ROS generation was observed by incubating HeLa cells with 300 μg mL^{-1} HA-loaded UCNPs@$mSiO_2$-PhL-PEG for 4 h and 50 μM dihydroethidium for 30 min at 37 °C, and then exposing the treated cells under 980-nm laser at 2 W cm^{-2} for 10 min to take the CLSM fluorescence images. HA-free UCNPs@$mSiO_2$-PhL-PEG was also tested as a control.

2.10. Endocytosis pathway of UCNPs

After HeLa cells were preincubated with different uptake inhibitors, genistein (200 μg mL^{-1}), wortmannin (50 nM), sucrose (450 mM) and NaN_3 (10 mM), for 30 min, the cells were incubated with siRNA-Cy5 and HA co-loaded UCNP nanocapsules to collect the CLSM images.

2.11. Endosomal escape of siRNA

The endosomal escape of siRNA was verified using siRNA-Cy5 loaded UCNPs@$mSiO_2$-PhL-PEG and LysoTracker Red to co-localize endosomal compartments. After the HeLa cells were incubated with 300 μg mL^{-1} siRNA-Cy5 and HA co-loaded UCNP nanocapsules for 4 h at 37 °C, and stained with 100 nM LysoTracker Red for 15 min, the NIR irradiation was conducted for 10 min to collect the CLSM images. HA-free UCNP nanocapsules loaded with siRNA-Cy5 were also tested as a control.

2.12. Gene silencing assay

After HeLa cells were seeded into a 24-well plate (Thermo Scientific Inc. US) at 5×10^5 cells per well and cultured for 24 h at 37 °C, 300 μg mL^{-1} siRNA-loaded, HA-loaded, and HA and siRNA co-loaded UCNP nanocapsules were added to the wells, incubated for 4 h, and exposed under NIR light for 80 min (with 10-min break after each 20-min irradiation). The cells were further cultured for 48 h to evaluate the cellular levels of PLK1 mRNA and protein using real-time quantitative PCR (RT-qPCR) and ELISA following the manufacturer's instructions. The gene silencing effect of UCNP nanocapsules were compared with those in the absence of NIR exposure or of commercial transfection agent Lipo2000 loaded with the same amount of siRNA.

To examine the heating effect of NIR light irradiation, 200 μL PBS was added into a 96-well plate at room temperature to measure the solution temperature upon 180-min NIR exposure (980 nm, 2 W cm^{-2}), or 1 mL DMEM was added into a 24-well plate at 36.4 °C to measure the solution temperature upon 80-min NIR exposure (980 nm, 2 W cm^{-2}).

2.13. Cell viability assay

After HeLa cells were cultured inside 96-well plate (Thermo Scientific Inc. US) with a culture density of 1×10^4 cells/chamber for 24 h, 300 μg mL^{-1} UCNPs loaded with different combination of HA and siRNA was added to each well to incubate for 4 h. After washing with PBS for two times, the cells were exposed under 980-nm light with a power density of 2 W cm^{-2} for 80 min (with 10-min break after each 20-min irradiation). These treated cells were then continuously cultured for 48 h to analyze the cell viability with MTT assay and flow cytometry. For flow cytometric analysis, the cells were stained with Annexin V-FITC/PI apoptosis detection kit.

2.14. In vivo antitumor efficiency

Pathogen-free female BALB/c nude mice (5–6 weeks) were purchased from Keygen Biotech (Nanjing, China), and all mice had liberated access to water and rodent chow. All experiments were conducted according to the Institutional Animal Use and Care Regulations approved by the Model Animal Research Center of Nanjing University (MARC). To establish a HeLa tumor xenograft mouse model, 1.0×10^6 HeLa cells were subcutaneously inoculated into the selected position of the female nude mice. The tumor volumes were calculated as $V = (L \times W^2)/2$, where L and W are the length and width of the tumor, respectively. When the tumor volumes reached 80 mm^3, the tumor-bearing mice were weighed and divided into six groups randomly. Afterward, different groups of mice were intratumorally injected with 150 μL of (1,2) saline, (3,4) siRNA-loaded UCNP nanocapsules (300 μg mL^{-1}), (5,6) HA and siRNA co-loaded UCNP nanocapsules (300 μg mL^{-1}). At 4 h after injection, the tumors on the mice of groups (1), (3) and (5) were irradiated with 980-nm laser at 1 W cm^{-2} for 40 min (10-min break for each 10-min exposure), while groups (2), (4) and (6) were not exposed to NIR light as controls. The injection and irradiation process was repeated at day 3 and day 6. The weight of the mice as well as the tumor sizes were recorded every 2 days. At Day 14, all mice were euthanized and representative gross photos of the mice

were taken.

3. Results and discussion

3.1. Preparation and characterization of UCNP nanocapsules

β-$NaYF_4$ crystalline structures co-doped with Tm^{3+} (0.5%) and Yb^{3+} (30%) were synthesized according to a previously reported solvent thermal method [44,48] and coated with $NaYbF_4$ shell to harvest more excitation photon and enhance the upconversion luminance [45]. The core-shell UCNPs were then encapsulated in a mesoporous silica shell ($mSiO_2$) with amine groups on its surface to facilitate further surface modification as well as photosensitizer and siRNA loading [46,47,49]. The obtained $NaYF_4$:Tm,Yb; $NaYF_4$:Tm,Yb@$NaYbF_4$ and UCNPs@$mSiO_2$ all showed the emission peaks corresponding to the $^1I_6 \rightarrow {}^3F_4$ and $^1D_2 \rightarrow {}^3H_6$ transitions of Tm^{3+} at 345 and 365 nm, the $^1D_2 \rightarrow {}^3F_4$ and $^1G_4 \rightarrow {}^3H_6$ transitions of Tm^{3+} at 455 and 475 nm, and the $^3H_4 \rightarrow {}^3H_6$ transition of Tm^{3+} at 805 nm (Fig. 1a) [50]. After coating $NaYbF_4$ shell, the core-shell UCNPs showed a dramatic increase of luminance intensity, while the coating of $mSiO_2$ resulted in the decrease of UCNP luminance to some extent. The successful coating of $NaYbF_4$ shell on core UCNPs was also evidenced by their size increase from 26 to 41 nm (Fig. 1b and c). The coating of mesoporous silica shell further increased its size to ~80 nm, which showed a uniform and homogenous mesoporous layer (Fig. 1d). The powder X-ray diffraction (XRD) patterns demonstrated that both core and core-shell UCNPs were hexagonal nanocrystals (Fig. S1), indicating that the $NaYbF_4$ coating did not change the lattice of $NaYF_4$:Tm,Yb. The mesoporous structure of $mSiO_2$ shell possessed a Brunauer-Emmett-Teller (BET) surface area of 700 $m^2\ g^{-1}$ and total pore volume of 0.76 $cm^3\ g^{-1}$ with a narrow Barret-Joyner/HAlenda (BJH) pore-size distribution (Fig. S2a). The average pore diameter was estimated to be 2.4 nm (Fig. S2b), which provided sufficient space for the subsequent loading of photosensitizer HA.

The synthesized PhL containing *o*-nitrobenzyl group (Scheme S1), which can be cleaved by UV light at 300–365 nm [51], was demonstrated by the relevant NMR spectra (Fig. S3). It could be easily attached to the UCNPs@$mSiO_2$ through aminoacylation reaction with surface amine groups, and the modified UCNPs showed the UV absorption band of PhL with a peak at 310 nm (Fig. S4a). The UV absorption band of PhL overlapped with the emission peaks of UCNPs at 345 and 365 nm (Fig. 2a, curves 1 and 3), thus the presence of PhL led to obvious decrease of these emission peaks (Fig. 2a, curve 2).

After the alkyne terminal group of PhL reacted with the azido terminal group at four arms of PEG, the PEG-tape wrapped UCNPs@$mSiO_2$-PhL-PEG was obtained. This reaction was confirmed using fluorescein isothiocyanate (FITC) functionalized PEG (PEGF) through the emission peak of FITC at 516 nm, which was covalently linked to UCNPs@$mSiO_2$-PhL surface with the same procedure (Fig. S4b). The absence of this emission peak for UCNPs@$mSiO_2$ after immersed in PEGF solution and then washed with water excluded the nonspecific adsorption of PEG on UCNPs@$mSiO_2$.

To achieve the targeted delivery of the UCNP nanocapsules into cells, folate acid labeled PEG (PEG(FA)) was mixed in the solution of PEG with azido terminal group to prepare the NIR responsive UCNP nanocapsules. The nanocapsules showed the IR absorption of FA at 1695 cm^{-1} and 1647 cm^{-1} for C=O bond stretching vibration of carboxyl group and C=O bond stretching vibration of –CONH– group respectively [52], while the characteristic peaks of PhL at 3272 cm^{-1} and 2121 cm^{-1} corresponding to the stretching

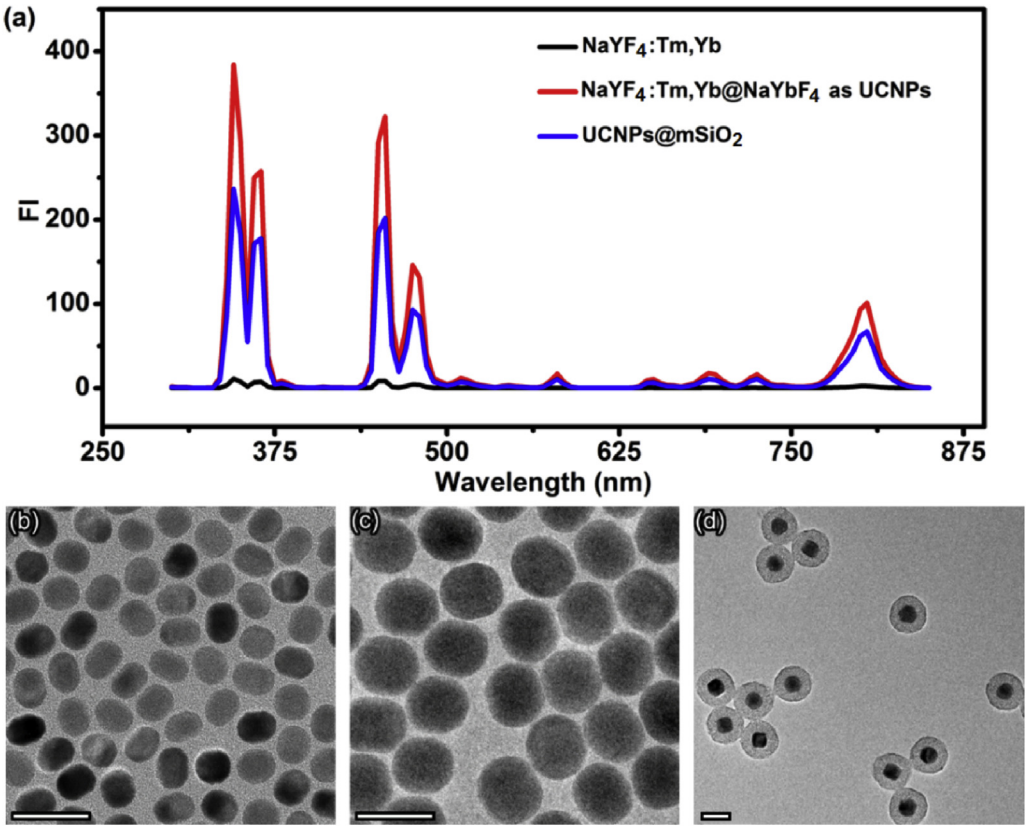

Fig. 1. Characterization of UCNPs and UCNPs@$mSiO_2$. (a) Upconversion luminescence spectra of $NaYF_4$:Tm,Yb; $NaYF_4$:Tm,Yb@$NaYbF_4$ and UCNPs@$mSiO_2$. TEM images of (b) $NaYF_4$:Tm,Yb, (c) $NaYF_4$:Tm,Yb@$NaYbF_4$ and (d) UCNPs@$mSiO_2$ (scale bar: 50 nm).

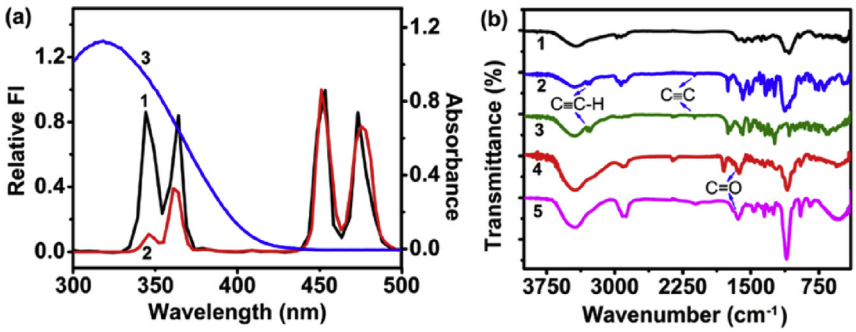

Fig. 2. Modification of PhL and PEG on UCNPs@mSiO$_2$. (a) Upconversion luminescence spectra of (1) UCNPs@mSiO$_2$, (2) UCNPs@mSiO$_2$-PhL and (3) UV–Vis absorption spectrum of PhL. (b) FT-IR spectra of (1) UCNPs@mSiO$_2$, (2) UCNPs@mSiO$_2$-PhL, (3) PhL, (4) UCNPs@mSiO$_2$-PhL-PEG(FA) and (5) PEG(FA).

vibration of C≡C–H and C≡C respectively disappeared due to the covalent linkage of PhL to PEG (Fig. 2b) [53,54]. After covalent linkage of PhL to PEG, the absorption peak of PhL at 1753 cm^{-1} for –NHCOO– group [55] shifted to 1799 cm^{-1} due to the steric-hindrance effect of the long-chain PEG. Though the wrapping of PEG polymer on UCNPs@mSiO$_2$-PhL did not result in its morphological change (Fig. 1d and Fig. S5), its size increased from 101 to 128 nm from DLS measurements (Figs. S4c and S4d), while the upconversion luminance intensity remained at the same value (Fig. S6).

3.2. SiRNA loading and photocontrollable release

The siRNA was loaded on the surface of UCNPs@mSiO$_2$-PhL *via* electrostatic interaction, and encapsulated by the PEG polymer tape. During this process, the zeta potential showed obviously changes (Fig. 3a). Upon the binding of PhL to UCNPs@mSiO$_2$, the zeta potential increased from 20.8 ± 5.3 mV to 32.4 ± 2.3 mV due to the aminoacylation reaction of PhL with surface amine groups [6] to bring alkynyl groups to the surface [56], which made the loading of negatively charged HA and siRNA much easier. The weak negative charge of HA slightly decreased the zeta potential from 32.4 ± 2.3 to 29.8 ± 2.1, while the relatively stronger negative charge of siRNA led to the zeta potential of −18.7 ± 1.3 mV. After the wrapping of the PEG tape, the zeta potential of siRNA loaded UCNPs@mSiO$_2$-PhL changed to −10.8 ± 2.2 mV. This process was further verified with 6-carboxyfluorescein (FAM) labeled siRNA. Upon its loading on UCNPs@mSiO$_2$-PhL, the characteristic emission peak of FAM could be observed at 515 nm (Fig. 3b). The wrapping of the PEG tape resulted in obvious decrease of the fluorescence intensity due to the

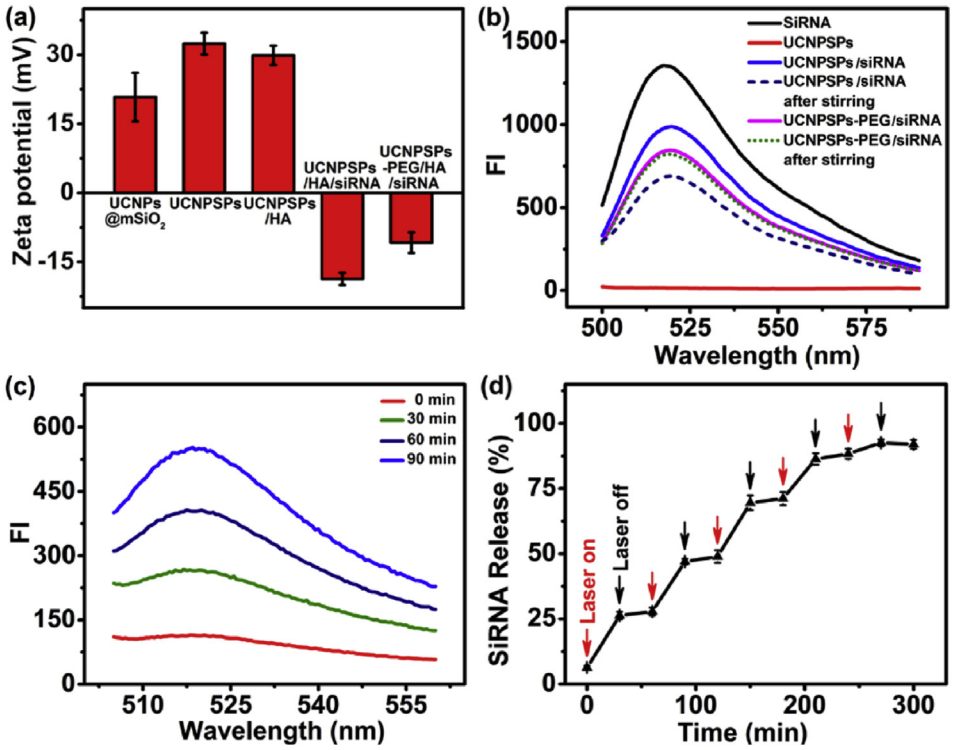

Fig. 3. Characterization of siRNA loading and release. (a) Zeta potentials of UCNPs@mSiO$_2$, UCNPSPs, UCNPSPs/HA, UCNPSPs/HA/siRNA and UCNPSPs-PEG/HA/siRNA. The error bars indicate means ± S.D. ($n = 3$). (b) Fluorescent luminescence spectra of marked materials. Here FAM labeled siRNA is marked as siRNA. (c) Fluorescent luminescence spectra of supernatant solutions collected from siRNA-FAM-loaded UCNP nanocapsules dispersions after NIR laser irradiation for 0, 30, 60 and 90 min and then centrifugation for 5 min. (d) Cumulative siRNA release from UCNP nanocapsules as a function of time under periodic irradiation with NIR laser on/off intervals of 30 min. The error bars indicate means ± S.D. ($n = 3$), and UCNPSPs is the abbreviate of UCNPs@mSiO$_2$-PhL.

detachment of some adsorbed siRNA during PEG encapsulation. However, the encapsulation made the adsorbed siRNA more stable on the surface, which was demonstrated from the stable fluorescence intensity upon stirring for 24 h. In contrast, the stirring led to larger decrease of the fluorescence of siRNA-FAM loaded UCNPs@mSiO$_2$-PhL. Thus PEG tape could protect siRNA from unintentional leakage.

To verify the serum stability of the loaded siRNA, a self-quenched siRNA duplex structure was synthesized by tagging FAM and black hole quencher (BHQ) to two complementary siRNA chains, respectively. After the duplex structure was loaded on UCNPs@mSiO$_2$-PhL and wrapped with PEG tape, the obtained UCNP nanocapsules showed very low fluorescence emission, and the fluorescence intensity increased by 34% after exposed to PBS containing 10% fetal bovine serum (FBS) over 12 h (Fig. S7). In contrast, the same exposure of the UCNP nanocapsules without presence of PEG led to the increase of fluorescence intensity by 246%, while the increase by 365% was observed for the self-quenched structure in the same solution. Therefore, the UCNP nanocapsules provided outstanding protection of loaded cargo against complicated intracellular conditions, which was necessary for efficient gene delivery and cancer therapy.

The photo-induced cleavage of PhL and tearing of the PEG tape were demonstrated by the UV adsorption of UCNPs@mSiO$_2$-PhL and the fluorescence emission of UCNP nanocapsules, respectively. With the increasing irradiation time at 980 nm, the adsorption of PhL centered at 310 nm from UCNPs@mSiO$_2$-PhL dispersed in pH 7.4 PBS gradually decreased, and the decomposition of PhL reached 80% after 180-min exposure (Fig. S8a), while the fluorescence from FITC labeled PEG (PEGF) of UCNPs@mSiO$_2$-PhL-PEGF at 516 nm greater decreased and almost disappeared at 180 min (Fig. S8b). As control, the temperature of pH 7.4 PBS at the same volume was measured upon its exposure to the same NIR light for 180 min, which increased the solution temperature from 23.4 °C to 31.1 °C (Fig. S9a). Obviously, the slight temperature increase could not tear off PEG tape from the UCNP nanocapsules, and the photo-induced cleavage of PhL led to tearing of the PEG tape.

To demonstrate the photo-induced controllable release of siRNA, siRNA-FAM loaded UCNP nanocapsules were exposed under NIR light for different times, and the supernatant solutions were collected for fluorescence measurements. The fluorescence intensity of FAM at 515 nm gradually increased with the increasing irradiation time due to the photocleavage of PEG (Fig. 3c), which led to the release of siRNA-FAM from the nanocapsules. The on-demand release could be monitored by continuously measuring the fluorescence intensity of supernatant solutions for 300 min during NIR irradiation with 30-min intervals and 5 cycles, which showed the alternate intensity increase (Fig. 3d), indicating that the amount of siRNA in the supernatant solution progressively rose up under NIR light exposure, while almost zero siRNA leakage was observed in the absence of NIR irradiation.

3.3. HA loading for ROS generation and endosomal escape of siRNA

Endosomal escape is a critical biological barrier for gene silencing [57]. Different strategies, including cell penetrating peptides [58], cationic polymers [59] and pH sensitive polymers [9], have been developed to facilitate endosomal escape. The photosensitizer-assisted endosomal escape of the intracellular delivered cargos has also been reported by generating ROS under irradiation to disrupt endosomal membrane [60,61]. In view of the overlap of efficient absorption of HA (~470 nm) with the emissions of UCNPs at 455 nm and 475 nm (Fig. 4a, curves 1 and 3) and its high photoquantum yield as well as super low dark toxicity [62], HA was chosen as the photosensitizer. The large surface area and pore volume of mesoporous silica shell enabled the high loading of HA [10], which led to the decrease of these emission peaks of UCNPs (Fig. 4a, curve 2). The HA loading was further confirmed by its characteristic absorption. The HA-loaded UCNPs@mSiO$_2$-PhL showed three absorption peaks of HA at 472 nm, 541 nm and 583 nm, which greatly decreased but remained the same intensity upon PEG wrapping after continuously stirring in PBS for 24 h (Fig. 4b), demonstrating the efficient encapsulation of HA *via* wrapping the PEG polymer tape.

The ROS generation upon NIR irradiation was determined by virtue of 1,3-diphenylisobenzofuran (DPBF), a sensing probe for ROS detection [63]. After the mixture of DPBF and HA-loaded UCNP nanocapsules was exposed under NIR light for different times, the supernatant solutions showed a continuous decrease of DPBF absorption peak at 412 nm due to the consumption of DPBF by the generated ROS (Fig. 5a and b). The ROS production in living cells was also investigated with dihydroethidium as a ROS detection probe, which can be oxidized by ROS to produce a red emission. As expected, the red emission could be observed under NIR irradiation (Fig. 5c), indicating the efficient generation of ROS intracellularly. Contrarily, the red emission did not appear in the cells treated with UCNP nanocapsules in the absence of HA (Fig. S10).

The co-staining experiment was performed to identify the HA-assisted escape of siRNA from endosomes. Endosomes were stained with LysoTracker Red and siRNA was labeled with cyanine-5 (siRNA-Cy5) to indicate their locations individually. The green (Cy5) and red (LysoTracker Red) fluorescence were well overlapped after 4-h incubation of HeLa cells with HA and siRNA-Cy5 co-loaded UCNP nanocapsules and staining with LysoTracker Red, (Fig. 6a, NIR (-)), indicating the loaded UCNP nanocapsules were stuck in endosomes [64]. After 10-min NIR irradiation, the Cy5 fluorescence spread in the entire cytoplasm due to the disruption of endosomes by generated ROS, while the LysoTracker Red fluorescence largely dimmed (Fig. 6a, NIR (+)), because its fluorescence was dependent on the low pH of endosomes, and the disruption resulted in raised pH of the microenvironment [4,65,66]. On the contrary, when HeLa cells were incubated with only siRNA-Cy5-loaded UCNP nanocapsules, the endosomal escape of siRNA upon 10-min NIR irradiation was not observed (Fig. 6b).

To evaluate the internalization pathway of UCNP nanocapsules into cells, HeLa cells were preincubated with a series of inhibitors to selectively block different internalization processes. Treatment of cells with NaN_3 and sucrose resulted in reductions of 64.5% and 54.9% in UCNP nanocapsules uptake, respectively (Fig. S11), indicating UCNP nanocapsules experienced mainly clathrin-dependent endocytosis pathway and sort of caveolae-dependent pathway upon entering the cells [67].

3.4. Gene silencing and cytotoxicity assay

The polo-like family of serine/threonine protein kinases (PLKs) has a significant impact on cell cycle regulation and proliferation [68,69], and PLK1 can promote oncogenic transformation [70]. Therefore inhibiting the expression of PLK1 may lead to cell cycle arrest, apoptosis, and mitotic catastrophe [71]. After HeLa cells were incubated with the UCNP nanocapsules for 4 h and irradiated under 980 nm for 80 min (10-min break between each 20-min exposure for 4 times), they were cultured for 48 h to determine the expression levels of PLK1 messenger RNA (mRNA) and PLK1 protein by real-time quantitative PCR (RT-qPCR) assay and enzyme-linked immunosorbent assay (ELISA) respectively. The siRNA-loaded UCNP nanocapsules down-regulated the PLK1 mRNA expression by 51.5% and PLK1 protein expression by 49.9%, while HA and siRNA co-loaded UCNP nanocapsules down-regulated their levels by 26.5% and 23.8%, respectively, which were lower than

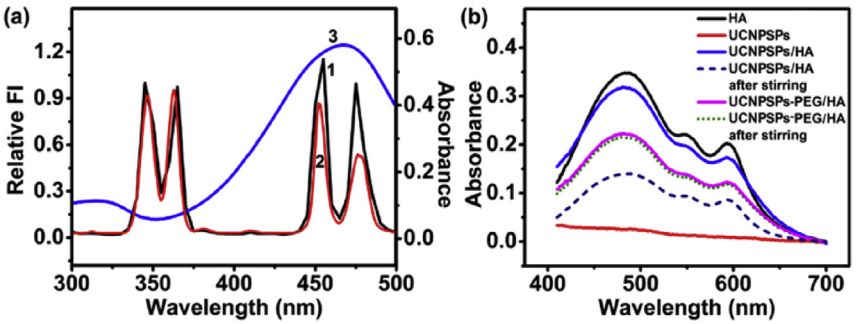

Fig. 4. Characterization of HA loading. (a) Upconversion luminescence spectra of (1) UCNPs@mSiO$_2$, (2) UCNPs@mSiO$_2$/HA and (3) UV–Vis absorption spectrum of HA. (b) UV–Vis absorption spectra of marked materials. Here UCNPs@mSiO$_2$-PhL is abbreviated as UCNPSPs.

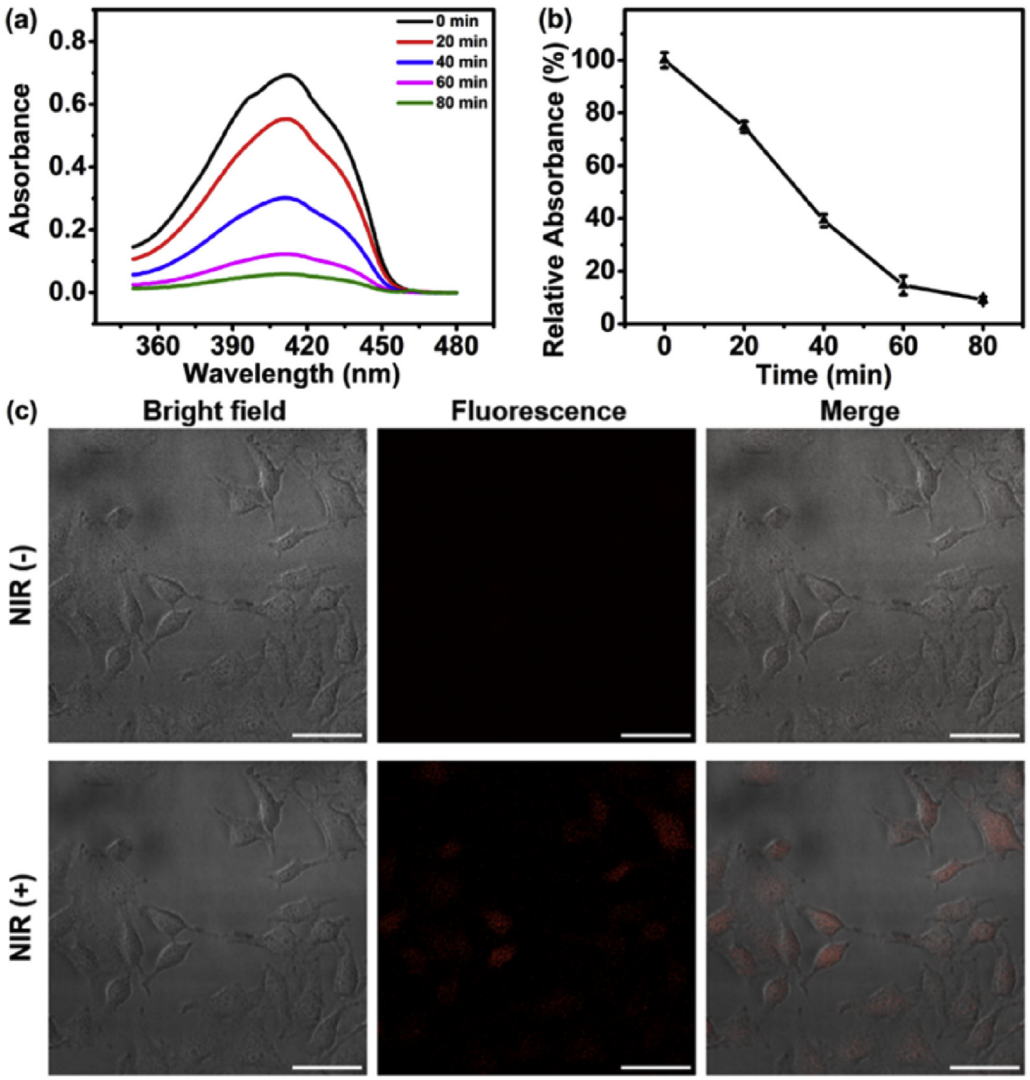

Fig. 5. ROS generation in solutions and HeLa cells. (a) UV–Vis absorption spectra and (b) relative UV–Vis absorbance percentage of supernatant DPBF solution at 412 nm after exposing UCNP nanocapsules under NIR laser irradiation for different times compared to that without irradiation. (c) Confocal microscopic images of HeLa cells treated with HA-loaded UCNP nanocapsules and then intracellular ROS detection probe before and after NIR laser irradiation (scale bar: 25 μm).

36.3% and 33.0% of commercial transfection reagent Lipofectamine 2000 (Lipo2000) (Fig. 7a and b), indicating more efficient inhibition of the UCNP nanocapsules to PLK1 expression, and the presence of HA resulted in significant difference ($^{*}P < 0.05$, $^{**}P < 0.01$). However, the HA and siRNA co-loaded UCNPs@mSiO$_2$-PhL only caused a moderate inhibition of 46.7% for PLK1 mRNA expression (Figs. 7a) and 44.6% for PLK1 protein expression due to the degradation of loaded siRNA (Fig. 7b), which demonstrated the outstanding contribution of the photo-tearable polymer tape PEG encapsulation. In the absence of NIR irradiation, the UCNP nanocapsules

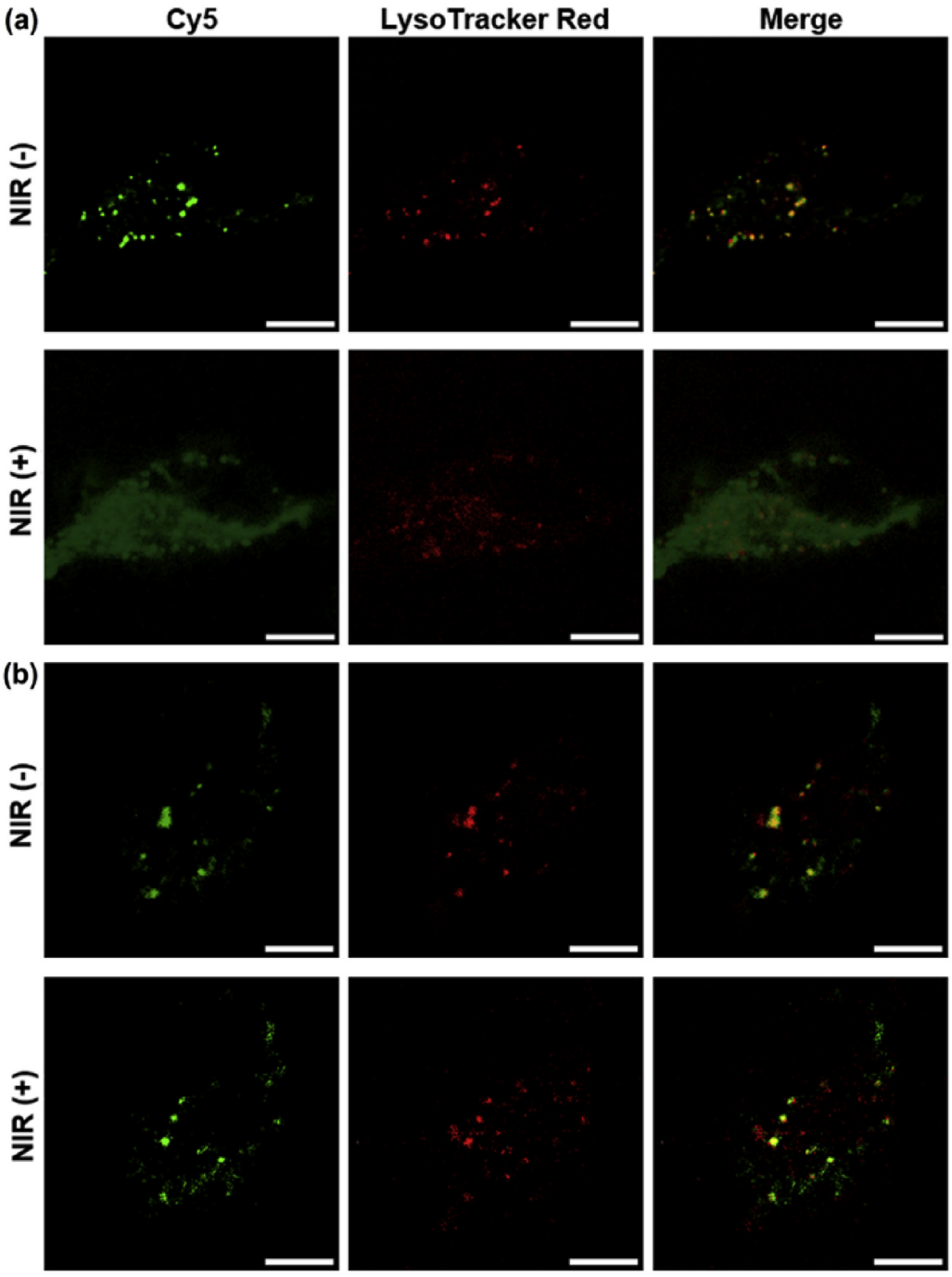

Fig. 6. Endosomal escape of siRNA in HeLa cells. Confocal microscopic images of HeLa cells incubated with (a) HA and siRNA-Cy5 co-loaded UCNP nanocapsules and (b) siRNA-Cy5-loaded UCNP nanocapsules and then stained with Lysotracker Red before and after NIR laser irradiation (scale bar: 7.5 μm).

showed little changes of both gene and protein expressions, while the HA and siRNA co-loaded UCNPs@mSiO_2-PhL showed the inhibition effects, suggesting that the PEG tape provided satisfactory biocompatibility and perfectly isolate the loaded HA and siRNA from cytoplasm.

3.5. Inhibition of cell proliferation

MTT assay was also used to verify the inhibition effect of UCNP nanocapsules to HeLa cell proliferation. Under NIR irradiation, the cells treated with siRNA and HA co-loaded UCNPs@mSiO_2-PhL-PEG nanocapsules showed a cell proliferation percentage of 25.7% compared with untreated cells, while the cells treated with the HA and siRNA co-loaded UCNPs@mSiO_2-PhL only showed 43.4% due to the desorption of loaded siRNA from the nanoparticles during the incubation (Fig. 7c). Thus the PEG-tape wrapped UCNPs@mSiO_2-PhL was an excellent carrier for siRNA delivery compared to the lower proliferation percentage of cancer cells than that of 36.1% for siRNA loaded Lipo2000 and the delivery of bare siRNA [72] due to the protection of PEG encapsulation and photo-controlled siRNA release. In the absence of photosensitizer HA, the cell proliferation percentage of the UCNP nanocapsules under NIR irradiation was

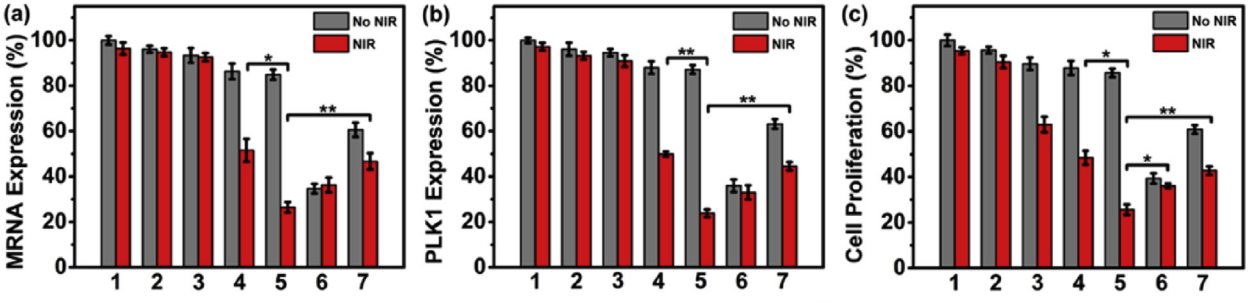

Fig. 7. Gene silencing and cell proliferation inhibition. Expression levels of (a) PLK1 mRNA detected with RT-qPCR and (b) PLK1 protein detected with ELISA, and (c) relative cell proliferation percentages for (1) HeLa cells as control and HeLa cells treated with (2) UCNPSPs-PEG, (3) UCNPSPs-PEG/HA, (4) UCNPSPs-PEG/siRNA, (5) UCNPSPs-PEG/HA/siRNA, (6) Lipo2000-siRNA and (7) UCNPSPs/HA/siRNA before and after NIR laser irradiation. Here UCNPs@mSiO_2-PhL is abbreviated as UCNPSPs. $^{*}P < 0.05$ and $^{**}P < 0.01$ with two-tailed Student's t-test. The error bars indicate means ± S.D. ($n = 3$).

48.3% (Fig. 7c). Considering the fact that the 5.8 °C increase of DMEM solution temperature upon 80-min NIR irradiation (Fig. S9b) could keep the cell proliferation percentage of 95.4% (column 1 in Fig. 7c), which showed 96.4% PLK1 mRNA expression and 97.2% PLK1 protein expression (column 1 in Fig. 7a and b), the ROS-assisted endosomal escape of siRNA and organelle destruction greatly boosted the inhibition effect. In the absence of NIR exposure, it did not show obvious proliferation inhibition for HeLa cells treated with PEG wrapped UCNP nanocapsules both with and without siRNA/HA loading (Fig. 7c).

Flow cytometric assay using the Annexin V-fluorescein isothiocyanate (FITC)/propidium iodide (PI) apoptotic kit showed similar phenomena. The UCNP nanocapsules did not harm HeLa cells in the absence of NIR laser, while 80-min NIR irradiation led to the maximum cell apoptosis of HeLa cells treated with the UCNP nanocapsules (Figs. S12h and S12e). The apoptosis rate of 69.7% was much higher than those of 31.5% and 45.0% for the cells treated with the UCNP nanocapsules loaded with only HA (Fig. S12c) and siRNA (Fig. S12d), respectively, and also higher than those of 60.1% for the cells treated with siRNA-loaded Lipo2000 and 53.0% for the cells treated with HA and siRNA co-loaded UCNPs@mSiO_2-PhL (Figs. S12f and S12g). These results demonstrated the feasibility of the photo-tearable UCNP nanocapsules as a promising approach for efficient anticancer therapeutics.

3.6. *In vivo* therapeutic applicability

Nude mouse was chosen as a model organism to demonstrate the *in vivo* antitumor efficacy of the PEG-tape wrapped UCNP nanocapsules. After saline, siRNA-loaded UCNP nanocapsules, and the proposed UCNP nanocapsules were intratumorally injected into these mice respectively for 40 min, the tumors were exposed under NIR irradiation of 1 W cm^{-2} for 40 min (10-min break for each 10-min exposure). The proposed UCNP nanocapsules presented pronounced inhibition efficacy towards tumor growth compared with saline solution control and siRNA-loaded UCNP nanocapsules ($^{**}P < 0.01$) (Fig. 8), suggesting that the co-loading of HA and siRNA could strongly enhance the gene therapeutic efficacy. All the mice groups (injected with saline, UCNPSPs-PEG/siRNA or UCNPSPs-PEG/HA/siRNA) treated without NIR irradiation did not show the suppression to tumor growth, which demonstrated the good photo-controllability of the UCNP nanocapsules. During the 14 days of experiment period, each group did not show obvious variation in their body weight (Fig. S13), indicating the satisfactory biocompatibility and specificity of these nanocapsules.

4. Conclusion

We design a photo-tearable tape-wrapped nanocapsule using UCNPs for siRNA delivery and controllable release, and present a strategy for efficient RNAi upon NIR modulation. The UCNPs ($NaYF_4$:Tm,Yb@$NaYbF_4$) are coated with a mesoporous silica shell to covalently link synthesized PhL for covalently wrapping the PEG polymer "tape". The siRNA and HA can be loaded on the surface of PhL modified silica *via* electrostatic adsorption and in the pores of mesoporous silica, respectively, and protected by PEG tape from leakage and/or degradation. The close attachment of PhL on silica shell improves the photocleavage efficiency of upconverted

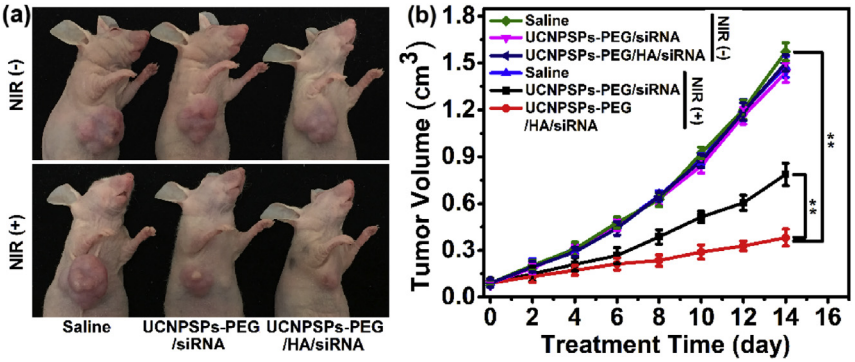

Fig. 8. *In vivo* antitumor therapy. Demonstration of therapeutic efficiency with (a) representative photos of xenograft tumors in mice at day 14 and (b) change of tumor volume as a function of time after treatment with marked materials. Here UCNPs@mSiO_2-PhL is abbreviated as UCNPSPs. $^{**}P < 0.01$ with two-tailed Student's t-test. The error bars indicate means ± S.D. ($n = 5$).

emissions for tearing off the PEG tape to release the loaded siRNA and HA. The intracellular generation of ROS not only assists endosomal escape of siRNA to boost the gene therapy efficiency, but also destructs organelles to prompt cell apoptosis. The photo-tearable tape-wrapped nanocapsules provide impressive improvement of RNAi efficiency to specifically inhibit cell proliferation and tumor growth *in vivo*, and thus show great importance for precise drug delivery and NIR-assisted tumor therapy.

Acknowledgements

This work was supported by the National Natural Science Foundation of China [21605083, 21635005, 21361162002]; Natural Science Foundation of Jiangsu Province [BK20160644]; and the National Research Foundation for Thousand Youth Talents Plan of China.

Appendix A. Supplementary data

Supplementary data related to this article can be found at https://doi.org/10.1016/j.biomaterials.2018.02.019.

References

[1] S.M. Elbashir, J. Harborth, W. Lendeckel, A. Yalcin, K. Weber, T. Tuschl, Duplexes of 21-nucleotide RNAs mediate RNA interference in cultured mammalian cells, Nature 411 (2001) 494–498.
[2] J. Conde, A. Ambrosone, Y. Hernandez, F. Tian, M. McCully, C.C. Berry, P.V. Baptista, C. Tortiglione, J.M. de la Fuente, 15 years on siRNA delivery: beyond the state-of-the-art on inorganic nanoparticles for RNAi therapeutics, Nano Today 10 (2015) 421–450.
[3] R. Kanasty, J.R. Dorkin, A. Vegas, D. Anderson, Delivery materials for siRNA therapeutics, Nat. Mater. 12 (2013) 967–977.
[4] K. Ren, Y. Liu, J. Wu, Y. Zhang, J. Zhu, M. Yang, H. Ju, A DNA dual lock-and-key strategy for cell-subtype-specific siRNA delivery, Nat. Commun. 7 (2016), 13580.
[5] H. Yin, R.L. Kanasty, A.A. Eltoukhy, A.J. Vegas, J.R. Dorkin, D.G. Anderson, Non-viral vectors for gene-based therapy, Nat. Rev. Genet. 15 (2014) 541–555.
[6] M.H. Kim, H.K. Na, Y.K. Kim, S.R. Ryoo, H.S. Cho, K.E. Lee, H. Jeon, R. Ryoo, D.H. Min, Facile synthesis of monodispersed mesoporous silica nanoparticles with ultralarge pores and their application in gene delivery, ACS Nano 5 (2011) 3568–3576.
[7] X. Huang, A. Pallaoro, G.B. Braun, D.P. Morales, M.O. Ogunyankin, J. Zasadzinski, N.O. Reich, Modular plasmonic nanocarriers for efficient and targeted delivery of cancer-therapeutic siRNA, Nano Lett. 14 (2014) 2046–2051.
[8] X. Xu, P.E. Saw, W. Tao, Y. Li, X. Ji, M. Yu, M. Mahmoudi, J. Rasmussen, D. Ayyash, Y. Zhou, O.C. Farokhzad, J. Shi, Tumor microenvironment-responsive multistaged nanoplatform for systemic RNAi and cancer therapy, Nano Lett. 17 (2017) 4427–4435.
[9] X. Xu, J. Wu, Y. Liu, P.E. Saw, W. Tao, M. Yu, H. Zope, M. Si, A. Victorious, J. Rasmussen, D. Ayyash, O.C. Farokhzad, J. Shi, Multifunctional envelope-type siRNA delivery nanoparticle platform for prostate cancer therapy, ACS Nano 11 (2017) 2618–2627.
[10] F. Tang, L. Li, D. Chen, Mesoporous silica nanoparticles: synthesis, biocompatibility and drug delivery, Adv. Mater. 24 (2012) 1504–1534.
[11] M.E. Davis, J.E. Zuckerman, C.H. Choi, D. Seligson, A. Tolcher, C.A. Alabi, Y. Yen, J.D. Heidel, A. Ribas, Evidence of RNAi in humans from systemically administered siRNA *via* targeted nanoparticles, Nature 464 (2010) 1067–1070.
[12] G. Lin, W. Zhu, L. Yang, J. Wu, B. Lin, Y. Xu, Z. Cheng, C. Xia, Q. Gong, B. Song, H. Ai, Delivery of siRNA by MRI–visible nanovehicles to overcome drug resistance in MCF-7/ADR human breast cancer cells, Biomaterials 35 (2014) 9495–9507.
[13] M. Antopolsky, M. Jafari, W. Xu, R. Pan, C.M. Sweeting, D.N. Karunaratne, P. Chen, Serum stability and physicochemical characterization of a novel amphipathic peptide C6M1 for siRNA delivery, PLoS One 9 (2014), e97797.
[14] M. Wu, Q. Meng, Y. Chen, Y. Du, L. Zhang, Y. Li, L. Zhang, J. Shi, Large-pore ultrasmall mesoporous organosilica nanoparticles: micelle/precursor co-templating assembly and nuclear-targeted gene delivery, Adv. Mater. 27 (2015) 215–222.
[15] N. Darwish, A.C. Aragones, T. Darwish, S. Ciampi, I. Diez-Perez, Multi-responsive photo- and chemo-electrical single-molecule switches, Nano Lett. 14 (2014) 7064–7070.
[16] S.S. Agasti, A. Chompoosor, C.C. You, P. Ghosh, C.K. Kim, V.M. Rotello, Photoregulated release of caged anticancer drugs from gold nanoparticles, J. Am. Chem. Soc. 131 (2009) 5728–5729.
[17] R. Wei, W. Xi, H. Wang, J. Liu, T. Mayr, L. Shi, L. Sun, *In situ* crystal growth of gold nanocrystals on upconversion nanoparticles for synergistic chemo-photothermal therapy, Nanoscale 9 (2017) 12885–12896.
[18] C. Brieke, F. Rohrbach, A. Gottschalk, G. Mayer, A. Heckel, Light-controlled tools, Angew. Chem. Int. Ed. 51 (2012) 8446–8476.
[19] S. Mura, J. Nicolas, P. Couvreur, Stimuli-responsive nanocarriers for drug delivery, Nat. Mater. 12 (2013) 991–1003.
[20] A.M. Kloxin, M.W. Tibbitt, K.S. Anseth, Synthesis of photodegradable hydrogels as dynamically tunable cell culture platforms, Nat. Protoc. 5 (2010) 1867–1887.
[21] G. Jalani, R. Naccache, D.H. Rosenzweig, L. Haglund, F. Vetrone, M. Cerruti, Photocleavable hydrogel-coated upconverting nanoparticles: a multifunctional theranostic platform for NIR imaging and on-demand macromolecular delivery, J. Am. Chem. Soc. 138 (2016) 1078–1083.
[22] G. Pasparakis, T. Manouras, M. Vamvakaki, P. Argitis, Harnessing photochemical internalization with dual degradable nanoparticles for combinatorial photo-chemotherapy, Nat. Commun. 5 (2014) 3623.
[23] R.M. Melero–Fernandez de Mera, L.L. Li, A. Popinigis, K. Cisek, M. Tuittila, L. Yadav, A. Serva, M.J. Courtney, A simple optogenetic MAPK inhibitor design reveals resonance between transcription-regulating circuitry and temporally-encoded inputs, Nat. Commun. 8 (2017), 15017.
[24] C. Wang, Q. Zhang, X. Wang, H. Chang, S. Zhang, Y. Tang, J. Xu, R. Qi, Y. Cheng, Dynamic modulation of enzyme activity by near-infrared light, Angew. Chem. Int. Ed. 56 (2017) 6767–6772.
[25] D. Bleger, S. Hecht, Visible-light-activated molecular switches, Angew. Chem. Int. Ed. 54 (2015) 11338–11349.
[26] L. Li, P. Hao, P. Wei, L. Fu, X. Ai, J. Zhang, J. Zhou, DNA-assisted upconversion nanoplatform for imaging-guided synergistic therapy and laser-switchable drug detoxification, Biomaterials 136 (2017) 43–55.
[27] D. Yang, P. Ma, Z. Hou, Z. Cheng, C. Li, J. Lin, Current advances in lanthanide ion (Ln^{3+})-based upconversion nanomaterials for drug delivery, Chem. Soc. Rev. 44 (2015) 1416–1448.
[28] N. Bogdan, F. Vetrone, G.A. Ozin, J.A. Capobianco, Synthesis of ligand-free colloidally stable water dispersible brightly luminescent lanthanide–doped upconverting nanoparticles, Nano Lett. 11 (2011) 835–840.
[29] J. Xu, Y. Kuang, R. Lv, P. Yang, C. Li, H. Bi, B. Liu, D. Yang, Y. Dai, S. Gai, F. He, B. Xing, J. Lin, Charge convertibility and near infrared photon co–enhanced cisplatin chemotherapy based on upconversion nanoplatform, Biomaterials 130 (2017) 42–55.
[30] C. Liu, Y. Zhang, M. Liu, Z. Chen, Y. Lin, W. Li, F. Cao, Z. Liu, J. Ren, X. Qu, A NIR-controlled cage mimicking system for hydrophobic drug mediated cancer therapy, Biomaterials 139 (2017) 151–162.
[31] L. Feng, F. He, B. Liu, G. Yang, S. Gai, P. Yang, C. Li, Y. Dai, R. Lv, J. Lin, G-C_3N_4 coated upconversion nanoparticles for 808 nm near-infrared light triggered phototherapy and multiple imaging, Chem. Mater. 28 (2016) 7935–7946.
[32] G. Yang, D. Yang, P. Yang, R. Lv, C. Li, C. Zhong, F. He, S. Gai, J. Lin, A single 808 nm near-infrared light-mediated multiple imaging and photodynamic therapy based on titania coupled upconversion nanoparticles, Chem. Mater. 27 (2015) 7957–7968.
[33] M.K. Jayakumar, N.M. Idris, Y. Zhang, Remote activation of biomolecules in deep tissues using near-infrared-to-UV upconversion nanotransducers, Proc. Natl. Acad. Sci. U. S. A 109 (2012) 8483–8488.
[34] J. Li, W.Y. Lee, T. Wu, J. Xu, K. Zhang, D.S. Hong Wong, R. Li, G. Li, L. Bian, Near-infrared light-triggered release of small molecules for controlled differentiation and long-term tracking of stem cells *in vivo* using upconversion nanoparticles, Biomaterials 110 (2016) 1–10.
[35] J. Xu, Y. Kuang, R. Lv, P. Yang, C. Li, H. Bi, B. Liu, D. Yang, Y. Dai, S. Gai, F. He, B. Xing, J. Lin, Charge convertibility and near infrared photon co-enhanced cisplatin chemotherapy based on upconversion nanoplatform, Biomaterials 130 (2017) 42–55.
[36] H.D. Gao, P. Thanasekaran, C.W. Chiang, J.L. Hong, Y.C. Liu, Y.H. Chang, H.M. Lee, Construction of a near-infrared-activatable enzyme platform to remotely trigger intracellular signal transduction using an upconversion nanoparticle, ACS Nano 9 (2015) 7041–7051.
[37] Q. Xiao, Y. Ji, Z. Xiao, Y. Zhang, H. Lin, Q. Wang, Novel multifunctional $NaYF_4$:Er^{3+},Yb^{3+}/PEGDA hybrid microspheres: NIR-light-activated photopolymerization and drug delivery, Chem. Commun. 49 (2013) 1527–1529.
[38] S. Beyazit, S. Ambrosini, N. Marchyk, E. Palo, V. Kale, T. Soukka, B. Tse Sum Bui, K. Haupt, Versatile synthetic strategy for coating upconverting nanoparticles with polymer shells through localized photopolymerization by using the particles as internal light sources, Angew. Chem. Int. Ed. 53 (2014) 8919–8923.
[39] Z. Cheng, J. Lin, Synthesis and application of nanohybrids based on upconverting nanoparticles and polymers, Macromol. Rapid Commun. 36 (2015) 790–827.
[40] B. Yan, J.C. Boyer, N.R. Branda, Y. Zhao, Near-infrared light-triggered dissociation of block copolymer micelles using upconverting nanoparticles, J. Am. Chem. Soc. 133 (2011) 19714–19717.
[41] B. Yan, J.C. Boyer, D. Habault, N.R. Branda, Y. Zhao, Near infrared light triggered release of biomacromolecules from hydrogels loaded with upconversion nanoparticles, J. Am. Chem. Soc. 134 (2012) 16558–16561.
[42] Y. Yang, F. Liu, X. Liu, B. Xing, NIR light controlled photorelease of siRNA and its targeted intracellular delivery based on upconversion nanoparticles, Nanoscale 5 (2013) 231–238.
[43] X. Ge, Z.M. Song, L. Sun, Y.F. Yang, L. Shi, R. Si, W. Ren, X. Qiu, H. Wang, Lanthanide (Gd^{3+} and Yb^{3+}) functionalized gold nanoparticles for *in vivo*

imaging and therapy, Biomaterials 108 (2016) 35–43.
[44] N. Wu, L. Bao, L. Ding, H. Ju, A single excitation-duplexed imaging strategy for profiling cell surface protein-specific glycoforms, Angew. Chem. Int. Ed. 55 (2016) 5220–5224.
[45] W. Shao, G. Chen, A. Kuzmin, H.L. Kutscher, A. Pliss, T.Y. Ohulchanskyy, P.N. Prasad, Tunable narrow band emissions from dye-sensitized core/shell/shell nanocrystals in the second near-infrared biological window, J. Am. Chem. Soc. 138 (2016) 16192–16195.
[46] C. Li, J. Liu, S. Alonso, F. Li, Y. Zhang, Upconversion nanoparticles for sensitive and in-depth detection of Cu^{2+} ions, Nanoscale 4 (2012) 6065–6071.
[47] B. Ruehle, D.L. Clemens, B.Y. Lee, M.A. Horwitz, J.I. Zink, A pathogen-specific cargo delivery platform based on mesoporous silica nanoparticles, J. Am. Chem. Soc. 139 (2017) 6663–6668.
[48] M.K. Gnanasammandhan, N.M. Idris, A. Bansal, K. Huang, Y. Zhang, Near-IR photoactivation using mesoporous silica-coated $NaYF_4$:Yb,Er/Tm upconversion nanoparticles, Nat. Protoc. 11 (2016) 688–713.
[49] S. Chai, Y. Guo, Z. Zhang, Z. Chai, Y. Ma, L. Qi, Cyclodextrin-gated mesoporous silica nanoparticles as drug carriers for red light-induced drug release, Nanotechnology 28 (2017), 145101.
[50] X. Li, F. Zhang, D. Zhao, Lab on upconversion nanoparticles: optical properties and applications engineering *via* designed nanostructure, Chem. Soc. Rev. 44 (2015) 1346–1378.
[51] H. Zhao, E.S. Sterner, E.B. Coughlin, P. Theato, *o*-Nitrobenzyl alcohol derivatives: opportunities in polymer and materials science, Macromolecules 45 (2012) 1723–1736.
[52] M.D. Howard, M. Jay, T.D. Dziubla, X. Lu, Poly(DL-lactide-*co*-glycolide) nanospheres for the sustained release of folic acid, J. Biomed. Nanotechnol. 4 (2008) 133–148.
[53] C. Yin, B. Hong, Z. Gong, H. Zhao, W. Hu, X. Lu, J. Li, X. Li, Z. Yang, Q. Fan, Y. Yao, W. Huang, Fluorescent oligo(*p*-phenyleneethynylene) contained amphiphiles-encapsulated magnetic nanoparticles for targeted magnetic resonance and two-photon optical imaging *in vitro* and *in vivo*, Nanoscale 7 (2015) 8907–8919.
[54] G. Temel, B. Aydogan, N. Arsu, Y. Yagci, Synthesis and characterization of one-component polymeric photoinitiator by simultaneous double click reactions and its use in photoinduced free radical polymerization, Macromolecules 42 (2009) 6098–6106.
[55] S.N. Rodrigues, I.M. Martins, I.P. Fernandes, P.B. Gomes, V.G. Mata, M.F. Barreiro, A.E. Rodrigues, Scentfashion®: microencapsulated perfumes for textile application, Chem. Eng. J. 149 (2009) 463–472.
[56] Y. Nishibayashi, M. Yoshikawa, Y. Inada, M. Hidai, S. Uemura, Ruthenium-catalyzed propargylation of aromatic compounds with propargylic alcohols, J. Am. Chem. Soc. 124 (2002) 11846–11847.
[57] D. Ma, Enhancing endosomal escape for nanoparticle mediated siRNA delivery, Nanoscale 6 (2014) 6415–6425.
[58] H. Zeng, H.C. Little, T.N. Tiambeng, G.A. Williams, Z. Guan, Multifunctional dendronized peptide polymer platform for safe and effective siRNA delivery, J. Am. Chem. Soc. 135 (2013) 4962–4965.
[59] C.E. Nelson, J.R. Kintzing, A. Hanna, J.M. Shannon, M.K. Gupta, C.L. Duvall, Balancing cationic and hydrophobic content of PEGylated siRNA polyplexes enhances endosome escape, stability, blood circulation time, and bioactivity *in vivo*, ACS Nano 7 (2013) 8870–8880.
[60] M.K. Jayakumar, A. Bansal, K. Huang, R. Yao, B.N. Li, Y. Zhang, Near-infrared-light-based nano-platform boosts endosomal escape and controls gene knockdown *in vivo*, ACS Nano 8 (2014) 4848–4858.
[61] Z. Guo, Y. Zou, H. He, J. Rao, S. Ji, X. Cui, H. Ke, Y. Deng, H. Yang, C. Chen, Y. Zhao, H. Chen, Bifunctional platinated nanoparticles for photoinduced tumor ablation, Adv. Mater. 28 (2016) 10155–10164.
[62] S. Jin, L. Zhou, Z. Gu, G. Tian, L. Yan, W. Ren, W. Yin, X. Liu, X. Zhang, Z. Hu, Y. Zhao, A new near infrared photosensitizing nanoplatform containing blue-emitting up-conversion nanoparticles and hypocrellin A for photodynamic therapy of cancer cells, Nanoscale 5 (2013) 11910–11918.
[63] X. He, X. Wu, K. Wang, B. Shi, L. Hai, Methylene blue-encapsulated phosphonate-terminated silica nanoparticles for simultaneous *in vivo* imaging and photodynamic therapy, Biomaterials 30 (2009) 5601–5609.
[64] Y.J. Ghang, M.P. Schramm, F. Zhang, R.A. Acey, C.N. David, E.H. Wilson, Y. Wang, Q. Cheng, R.J. Hooley, Selective cavitand-mediated endocytosis of targeted imaging agents into live cells, J. Am. Chem. Soc. 135 (2013) 7090–7093.
[65] R. Mo, T. Jiang, R. DiSanto, W. Tai, Z. Gu, ATP-triggered anticancer drug delivery, Nat. Commun. 5 (2014) 3364.
[66] S.–j. Park, W. Park, K. Na, Tumor intracellular-environment responsive materials shielded nano-complexes for highly efficient light-triggered gene delivery without cargo gene damage, Adv. Funct. Mater. 25 (2015) 3472–3482.
[67] G. Chen, D. Liu, C. He, T.R. Gannett, W. Lin, Y. Weizmann, Enzymatic synthesis of periodic DNA nanoribbons for intracellular pH sensing and gene silencing, J. Am. Chem. Soc. 137 (2015) 3844–3851.
[68] F. Liu, J.E. Park, W.J. Qian, D. Lim, M. Graber, T. Berg, M.B. Yaffe, K.S. Lee, T.R. Burke Jr., Serendipitous alkylation of a Plk1 ligand uncovers a new binding channel, Nat. Chem. Biol. 7 (2011) 595–601.
[69] F.A. Barr, H.H. Sillje, E.A. Nigg, Polo–like kinases and the orchestration of cell division, Nat. Rev. Mol. Cell Biol. 5 (2004) 429–440.
[70] K. Strebhardt, A. Ullrich, Targeting polo-like kinase 1 for cancer therapy, Nat. Rev. Canc. 6 (2006) 321–330.
[71] L. Zhang, W. Zheng, R. Tang, N. Wang, W. Zhang, X. Jiang, Gene regulation with carbon-based siRNA conjugates for cancer therapy, Biomaterials 104 (2016) 269–278.
[72] R. van der Meer, H.Y. Song, S.H. Park, S.A. Abdulkadir, M. Roh, RNAi screen identifies a synthetic lethal interaction between PIM1 overexpression and PLK1 inhibition, Clin. Canc. Res. 20 (2014) 3211–3221.